12 Bridges

12.1 Introduction

As discussed in Chapter 1, bridges have featured in some spectacular failures during wind storms (Figure 1.10). The history of the dynamically wind-sensitive suspension bridge from the nineteenth century onwards, including the periodic failures that have occurred, has been well documented (e.g. Steinman and Watson, 1957; Billington, 1977; Petroski, 1996).

Most of the early interest was in the drag, or along-wind forces, and Baker (1884), Kernot (1893) and others, noted that peak wind forces acting on large areas, such as a complete bridge girder, were considerably less than those on a small plate or board. However, the great American builder of suspension bridges John Roebling, was aware of the dynamic effects of wind as early as 1855. In commenting on the failure of the Wheeling Bridge, Ohio, in the previous year, he wrote: 'That bridge was destroyed by the momentum acquired by its own dead weight, when swayed up and down by the force of the wind…. A high wind, acting upon a suspended floor, devoid of inherent stiffness, will produce a series of undulations, which will be corresponding from the center each way', (Steinman and Watson, 1957).

However, it took over 80 years for the dramatic failure of the first Tacoma Narrows suspension bridge in 1940 (Section 1.4), to direct serious attention to the the dynamic actions of the wind, and other wind actions on bridge decks: vertical cross-wind forces, and torsional moments.

The cable-stayed bridge emerged in the 1950s in Germany, as an efficient method of spanning intermediate length crossings. Gimsing (1983) and Virlogeux (1999) have reviewed recent developments in the design of bridges of this type.

As the twentieth century ends, the spans of the long-span suspension and cable-stayed bridges have been extended to new limits. The longest bridge in the world at the turn of the century is the suspension bridge across the Akashi-Kaikyo Straits in Japan, which has an overall length of nearly 4 km, with a main span of 1990 m (Figure 12.1). The design of this bridge was dominated by its aerodynamic characteristics.

The longest cable-stayed bridge is the Tatara Bridge, also in Japan, with an overall length of 1480 m, and a main span of 890 m (Figure 12.2).

As the spans increase, wind actions become more critical in bridge design, and for the longest suspension or cable-stayed bridges, extensive wind studies are normally undertaken. The dynamic wind forces will excite resonant response, often in several modes, and *aeroelastic* forces, in which the motion of the structure itself generates forces, are important. Long-span bridges are usually crossings of large expanses of water, and may be exposed to relatively low-turbulence flow, at least at low wind speeds. This has contributed to a number of cases of vibrations of bridge decks induced by vortex shedding (Section 4.6.3). Recently the spans of cable-stayed bridges have been limited by problems with cable vibrations, sometimes involving rain, as well as wind (Section 12.5).

Figure 12.1 Akashi-Kaikyo Bridge, Japan.

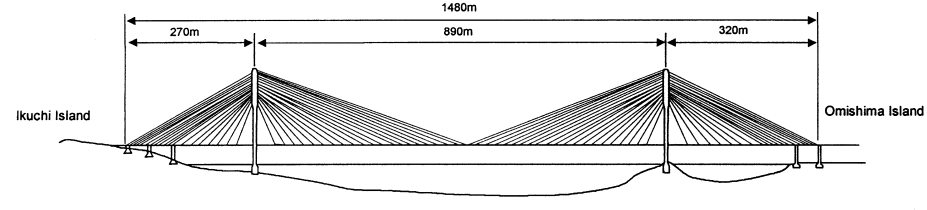

Figure 12.2 Tatara Bridge, Japan.

In the following sections, a review of the main aspects of wind forces and the wind-induced excitation of long-span bridges, and their supporting cables is given. The aerodynamics of bridges is a large and specialist topic, and an in-depth treatment will not be given in this book. The reader is referred to other sources (e.g. Larsen, 1992; Simiu and Scanlan, 1996) which treat the subject in more detail.

12.2 Basic force coefficients for bridges

As for other structures, all bridges are subjected to mean and fluctuating wind forces. These may be estimated by the use of mean, or steady state, force coefficients, usually determined from wind tunnel tests. Such coefficients are also required to determine dynamic response from turbulent buffeting.

Many wind tunnel section tests of decks for long-span bridges (Section 7.6.3) have been carried out, primarily to determine their aerodynamic stability (Section 12.3.2). Determi-

nation of the basic section force coefficients, as a function of wind angle of attack, is also routinely done during the tests.

Most nineteenth century suspension bridges were built with open-lattice truss sections. This use has continued, as this type of section has some benefits from the point of view of dynamic response. The open structure prevents the formation of vortices, and dynamic excitation from vortex shedding (Section 4.6.3) is not usually a problem. Provided the torsional stiffness can be made high enough, the critical speed for flutter instability (Sections 5.5.3 and 12.3.2) will be high. However, the drag coefficients for open-truss sections are high in comparison with other sections. For example, the drag coefficients for two cross-sections considered for the Little Belt suspension bridge completed in the 1960s in Denmark, are shown in Figure 12.3 (Ostenfeld and Larsen, 1992). The drag coefficient for the trussed cross-section is more than three times that of the streamlined box girder section; the latter was eventually used for the bridge. However, after extensive aerodynamic testing (Miyata *et al.*, 1993), a truss girder, 11 m deep, was chosen for the Akashi-Kaikyo suspension bridge – the world's longest (Figure 12.1).

Note that the along-wind *chord* dimension, *d*, rather than the cross-wind dimension, *b*, has been used to define the drag coefficients. This is usually the convention for bridges.

Very slender deck cross-sections, such as the box girder section shown in Figure 12.3,

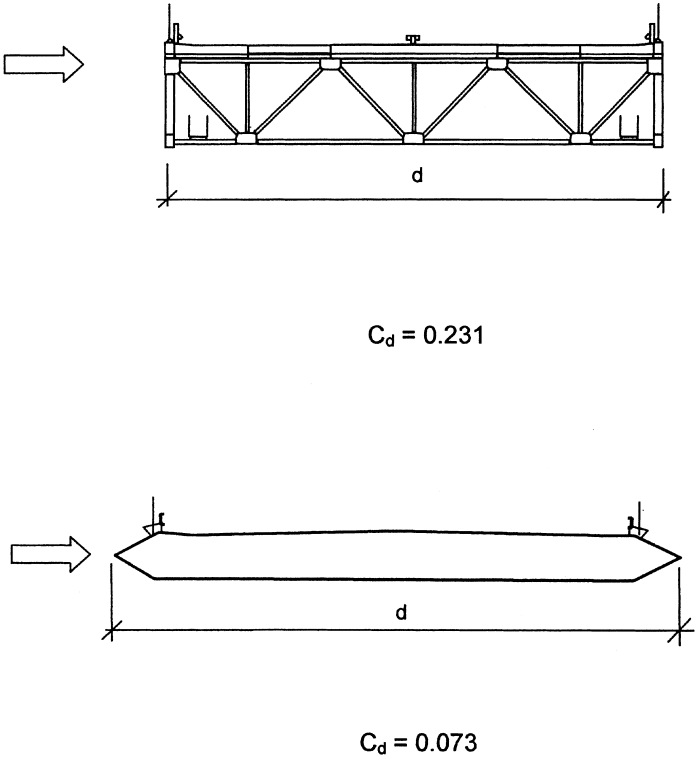

Figure 12.3 Comparison of drag coefficients for two bridge deck cross-sections (Ostenfeld and Larsen, 1992), (reproduced by permission from 'Aerodynamics of large bridges' – Proceedings of the First International Symposium, Copenhagen, 19–21 February, 1992, Larsen, Allan (ed.)).

although having very low drag coefficients, will have high lift (cross-wind) force coefficients (Section 4.2.2) when the wind has a significant angle of attack, in a similar way to an airfoil. This situation will occur instantaneously in turbulent flow. This characteristic makes deck sections of this type prone to buffeting by vertical turbulence (Section 12.3.3).

Examples of the variation of static horizontal and vertical force coefficients, and moment coefficient about the mass centre of a bridge deck section, with angle of attack, are given in Figure 12.4.

The conventional definition of section force and pitching moments for bridges is as follows:

$$C_X = \frac{F_x}{\frac{1}{2}\rho_a U^2 d} \qquad C_Z = \frac{F_z}{\frac{1}{2}\rho_a U^2 d} \qquad C_M = \frac{M}{\frac{1}{2}\rho_a U^2 d^2} \tag{12.1}$$

12.3 The nature of dynamic response of long-span bridges

There are several mechanisms, in various wind speed ranges, which can excite resonant dynamic response in the decks of long-span bridges, as follows.

- Vortex shedding excitation (Section 4.6.3) which usually occurs in low wind speeds and low turbulence conditions (e.g. Frandsen, 2001).
- Flutter instabilities (Section 5.5.3) of several types, which occur at very high wind speeds for *aerodynamically stable* decks, as a result of the dominance of self-excited

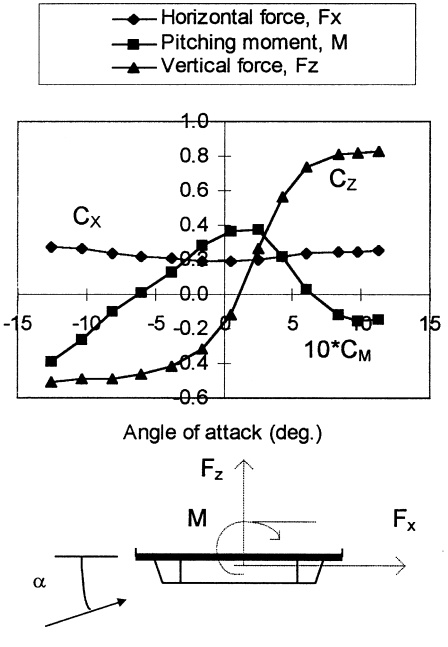

Figure 12.4 Static force coefficients for a typical bridge deck section.

aerodynamic forces (Sabzevari and Scanlan, 1968). These always involve torsional (rotational) motions, and may also involve vertical bending motions.
- Buffeting excitation (Section 4.6.1) caused by the fluctuating forces induced by turbulence (Davenport, 1962; Scanlan and Gade, 1977). This occurs over a wide range of wind speeds, and normally increases monotonically with increasing wind speed.

The nature of these mechanisms is discussed in the following sections.

12.3.1 Vortex-shedding excitation

Under certain conditions, vortex-shedding excitation can induce significant, but limited, amplitudes of vibration. The conditions required for this to occur are most, or all, of the following:

- Wind direction normal to the longitudinal axis of the bridge
- Low turbulence conditions (typically I_u less than 0.05)
- A wind speed in a narrow critical range (5–12 m/s)
- Low damping (1% of critical or less)

The above conditions can be satisfied for both short to medium span cable-stayed bridges crossing water, and longer span suspension bridges. With Strouhal numbers in the range of 0.1 to 0.2 (based on the depth of the deck cross-section), and natural frequencies in the range of 0.1 to 0.6 Hz, critical velocities of 6 to 15 m/s can produce significant amplitudes. Low turbulence conditions can occur in 'stable' atmospheric conditions, often in the early morning or evening. Recorded examples of this behaviour are listed in Table 12.1.

Section tests carried out in smooth flow in wind tunnels can provide reasonably good predictions of the full-scale behaviour (Wardlaw, 1971; van Nunen and Persoon, 1982). In the case of the Long's Creek Bridge, Canada, where the vibrations were large enough to require remedial action, triangular fairings on the ends, and a soffit plate underneath the deck were added to the prototype structure, with satisfactory results (Wardlaw, 1971). Guide vanes were used at the lower corners of the box girder of the Great Belt East suspension bridge, a method known to be successful in suppressing vortex shedding vibrations, which occurred at four different frequencies and a corresponding wide range of wind speeds. Lock-in effects (Sections 4.6.3 and 5.5.4) were also observed in the vortex-induced vibration on this bridge (Frandsen, 2001).

Table 12.1 Some recorded cases of vortex-shedding induced vibrations of bridges

Name	*Natural frequency (Hz)*	*Critical velocity (m/s)*	*Max. amplitude (mm)*	*Reference*
Long's Creek Bridge	0.6	12	100–170	Wardlaw (1971)
Wye Bridge	0.46	7.5	35	Smith (1980)
Waal River	0.44	9–12	50	van Nunen and Persoon (1982)
Great Belt East	0.13–0.21	4.5–9	320	Larsen *et al.* (1999) Frandsen (2001)

12.3.2 *Flutter instabilities and prediction of flutter speeds*

The coupled motion (rotation and vertical displacement) of a suspended bluff body was discussed in Section 5.5.3. Equations (5.42) and (5.43) – the coupled equations of motion – are repeated as follows:

$$\ddot{z} + 2\eta_z\omega_z\dot{z} + \omega_z{}^2 z = \frac{F_z(t)}{m} + H_1\dot{z} + H_2\dot{\theta} + H_3\theta \tag{5.42}$$

$$\ddot{\theta} + 2\eta_\theta\omega_\theta\dot{\theta} + \omega_\theta{}^2\theta = \frac{M(t)}{I} + A_1\dot{z} + A_2\dot{\theta} + A_3\theta \tag{5.43}$$

Equations (5.42) and (5.43) are simplified forms of the full equations of motion, which include the horizontal motions of the deck, and as many as eighteen different aeroelastic derivatives, corresponding to all possible motion-induced forces. Many of these terms are small, however. The propensity of a bridge deck to flutter instability depends on the magnitudes and signs of some of the aeroelastic derivatives, or *flutter derivatives*, of the particular deck cross-section as a function of the wind speed. For example, a positive value of the derivative, A_2 is an indication of flutter in a pure rotational motion – sometimes known as 'stall flutter' in aeronautical terminology. This can be seen from equation (5.43) when the term $A_2\dot{\theta}$ is transposed to the left-hand-side of the equation – it then has the form of a negative damping term, with the ability to *extract* energy from the flow. If the magnitude of the negative aerodynamic is greater than the structural damping, then vibrations will grow in amplitude – i.e. an aeroelastic instability will occur.

The most commonly understood use of the term 'flutter' however is to describe the coupled translational-rotational form of instability which is largely governed by the signs of the derivatives H_2 and A_1 (see Table 5.1).

Data on the flutter derivatives A_i to H_i is usually obtained experimentally from section tests in wind tunnels (see Section 7.6.3). Tests are usually done in smooth (low turbulence) flow – it has been found that the effects of turbulence on the derivatives are generally small (Scanlan and Lin, 1978). The derivatives are a function of reduced velocity, $\left(\frac{U}{nd}\right)$ which incorporates the variation with frequency of vibration, n, as well as the wind speed, U. The following non-dimensional forms are usually used for the derivatives (Scanlan and Tomko, 1971).

$$H_1^* = \frac{mH_1}{\rho_a d^2\omega};\ A_1^* = \frac{IA_1}{\rho_a d^3\omega}$$

$$H_2^* = \frac{mH_2}{\rho_a d^3\omega};\ A_2^* = \frac{IA_2}{\rho_a d^4\omega}$$

$$H_3^* = \frac{mH_3}{\rho_a d^3\omega^2};\ A_3^* = \frac{IA_3}{\rho_a d^4\omega^2} \tag{12.2}$$

where m and I are the mass and moment of inertia per unit length (spanwise), d is the width (chord) of the deck, ρ_a is the air density, and ω is the circular frequency ($=2\pi n$).

Examples of aeroelastic derivatives determined for two common types of bridge deck – an open truss and a box-girder – are shown in Figure 12.5.

Although the magnitude and sign of the derivatives give some indication of the tendency of a particular section to aerodynamic instability, in the design stage of important long-span bridges, it is usual to attempt to determine a 'critical flutter speed' for the deck cross-section. If this wind speed does not exceed, by a substantial margin, the design wind speed of the site at the deck height (suitably factored for ultimate limit states), then modifications to the deck cross-section are usually made.

Several methods may be used to determine the critical flutter speed:

- empirical formulae (e.g. Selberg, 1963)
- experimental determination by use of section model testing
- theoretical stability analysis of the equations of motion (equations (5.42) and (5.43)), with values of A_i and H_i obtained experimentally (e.g. Simiu and Scanlan, 1996)

Selberg (1963) proposed an empirical equation for critical flutter speed, U_F, which, in its simplest form, can be written as equation (12.3).

$$U_F = 0.44d\sqrt{(\omega_T^2 - \omega_V^2)\frac{\sqrt{\nu}}{\mu}} \tag{12.3}$$

where $\nu = 8\left(\frac{r}{d}\right)^2$ and $\mu = \frac{\pi\rho_a d^2}{4m}$; r is the radius of gyration of the cross-section ($I = mr^2$); ω_T ($=2\pi n_T$) and ω_V ($=2\pi n_V$) are the circular frequencies in the first torsional mode and first vertical bending modes, respectively.

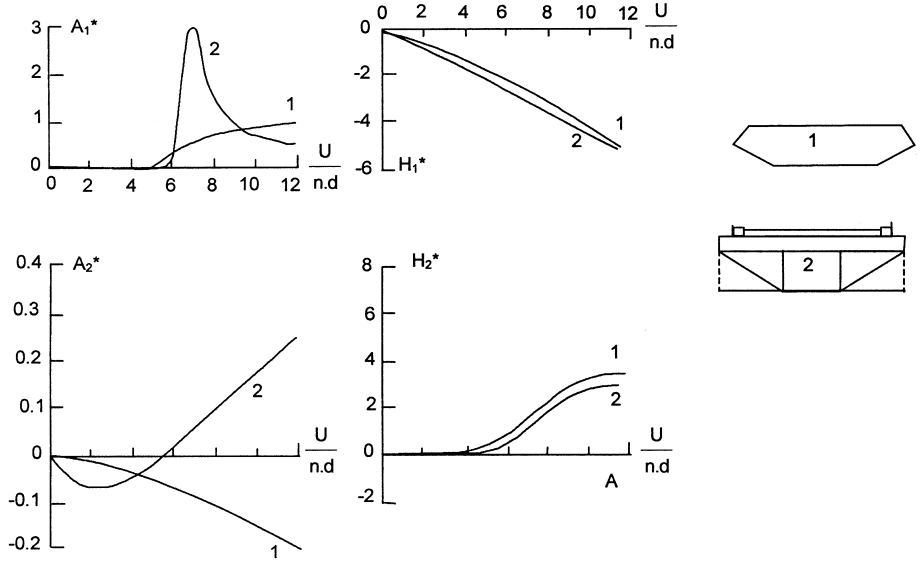

Figure 12.5 Aeroelastic derivatives for two types of bridge deck (Scanlan and Tomko, 1971).

Figure 12.6 shows measured flutter speeds for several bridge deck sections compared with predictions from the Selberg formula. Reasonable agreement is obtained although there is an overestimation at low angles of attack. It would appear to be unwise to rely on a prediction based on an empirical formula alone.

The analytical estimation of flutter speeds is a specialist function of bridge aerodynamicists, but Ge and Tanaka (2000) have given a useful summary of the techniques available.

12.3.3 Buffeting of long-span bridges

A bridge that is otherwise stable in flutter up to a high wind speed, and does not suffer from vortex-induced vibrations at low wind speeds, will still experience dynamic response to atmospheric turbulence, known as *buffeting* over a wide range of wind speeds. This response will normally determine the size of the structural members and require evaluation at the design stage.

Davenport (1962) was the first to apply random vibration methods to the buffeting of a long-span suspension bridge. These methods were later validated by comparison with model studies in turbulent boundary layer flow in the 1970s (e.g. Holmes, 1975, 1979; Irwin, 1977).

The methodology described in Section 5.3.6 for the along-wind response of distributed mass structures can be adapted to the *cross*-wind response of bridge decks excited by vertical turbulence components.

The sectional cross-wind force per unit span can be written applying a 'strip' assumption:

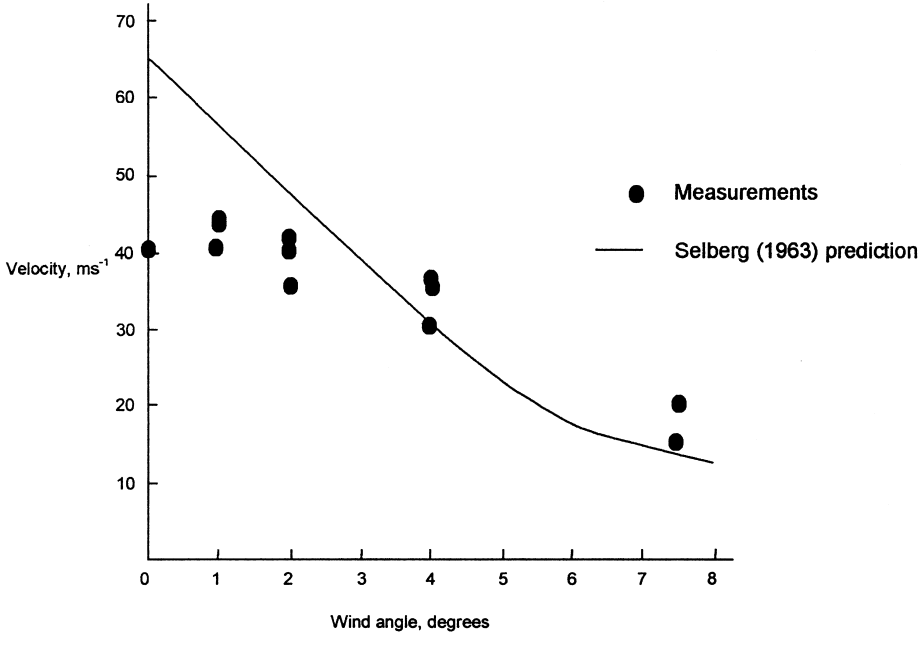

Figure 12.6 Measured critical flutter speeds and comparisons with the Selberg prediction formula (Wardlaw, 1971).

$$f'(z,t) = \rho_a \bar{U} d[C_{Zo} u'(t) + \frac{1}{2}\frac{dC_Z}{d\alpha} w'(t)] \tag{12.4}$$

where C_{Zo} is the vertical force coefficient at zero angle of attack; $\frac{dC_Z}{d\alpha}$ is the slope of the vertical force coefficient versus angle of attack, α; $u'(t)$ and $w'(t)$ are the horizontal and vertical velocity fluctuations upstream of the deck section in question.

C_{Zo} and $\frac{dC_Z}{d\alpha}$ can be obtained from static section tests of the deck cross-section (Section 12.2). If there is significant angular rotation of the bridge deck under the mean wind load (as is often the case with suspension bridges), then C_{Zo} may need to be replaced by the value of C_Z at the mean (non-zero) angle of attack under the mean wind loading.

Following an argument similar to that used in Section 5.3.6, the spectral density of the generalized force for the jth mode of vibration can be obtained.

$$S_{Qj}(n) = (\rho_a \bar{U} d)^2 \left[C_{Zo}^2 S_u(n) + \frac{1}{4}\left(\frac{dC_Z}{d\alpha}\right)^2 S_w(n) \right] \chi^2(n) \int_0^L \int_0^L \rho(y_1, y_2, n) \phi_j(y_1) \phi_j(y_2) \; dy_1 \; dy_2 \tag{12.5}$$

In equation (12.5), $\chi^2(n)$ is an *aerodynamic admittance*, allowing for the fact that smaller gusts (higher frequencies) do not completely envelope the bridge cross-section. Konishi *et al.* (1975), Shiraishi and Matsumoto (1977), Jancauskas (1986) and others have directly measured this function for bridge deck sections and other bluff shapes. Note that this aerodynamic admittance which applies to vertical (cross-wind) aerodynamic forces) is similar, but not identical, to that discussed in Section 5.3.1, which relates to along-wind forces, and response.

Analysis based on equation (12.5) and the methods of random vibration analysis outlined in Section 5.3.6, have given good agreement with the measured response on full aeroelastic wind tunnel models (e.g. Holmes, 1975) and full-scale measurements (Melbourne, 1979). However, for large span bridges, the towers and cables play important parts in the overall bridge response, and it is the practice to carry out full aeroelastic model studies in simulated turbulent boundary-layer flow, as described in Section 12.4.

12.3.4 Effective static load distributions

The method of equivalent static load distributions discussed in Section 5.4 can be applied to the response of bridges. In many cases of long span bridges, the background response can be neglected in comparison to the resonant contributions. However, it is often the case that several modes are significant. The following approach (Holmes, 1999) gives the correct method of combining inertial force distributions from more than one resonant mode of vibration. This approach is consistent with the weighting factor method discussed in Section 5.4.5.

The mean square fluctuating value of a load effect, r, resulting from the resonant response in mode j, can be written:

$$\sigma_{rj}^2 = \alpha_j^2 \omega_j^4 \overline{a_j^2} \tag{12.6}$$

where the displacement response of the deck is written as:

$$y\,(x,t) = \phi_j(x).\, a_j(t)$$

$\phi_j(x)$ is the mode shape, and $a_j(t)$ is the modal coordinate for the jth mode; ω_j is the circular frequency in mode $j(=2\pi n_j)$, α_j is the integral:

$$\int_0^L m(x).\phi_j(x).I(x)dx \tag{12.7}$$

$m(x)$ is the mass per unit length, and $I(x)$ is the influence line for the load effect in question.

The contribution of the load at each spanwise position to the load effect, is the product of the inertial load on a small increment of span, centred at that position, $m(x).\omega_j^2\,.y(x,t).\delta x$, multiplied by the influence function, $I(x)$. Equation (12.6) is then obtained by integration of the contributions over the span, L, squaring and taking the mean value.

The *total* mean square fluctuating response is then obtained by summing the contributions from the N contributing modes.

$$\sigma_r^2 = \sum_j^N \alpha_j^2 \omega_j^4 \overline{a_j^2} \tag{12.8}$$

To obtain equation (12.8), we have assumed that the modes are well separated, and hence the resulting responses can be assumed to be uncorrelated with each other.

The *envelope* of the combined dynamic loadings at each point along the span of a bridge, can be obtained by taking the root sum of squares of the inertial loads from the contributing modes along the span, and adding to the mean loading. Thus,

$$f_{\text{env}}(x) = \bar{f}(x) \pm \left[\sum_j^N (m(x).\omega_j^2 \phi_j(x))^2 \overline{a_j^2} \right]^{1/2} \tag{12.9}$$

where $\bar{f}(x)$ is the mean wind loading at x.

Note that the envelope is independent of the influence line $I(x)$ of the load effect. It represents the limits within which the effective static load distributions for all load effects must lie.

The contribution of each mode to the total static equivalent load corresponding to a peak load effect (e.g. a bending moment at any point along the span) depends on the shape of the influence line for that load effect. Thus there is not a single static equivalent load. The weighting factor to be applied to obtain the contribution from mode j to the combined inertial load for a *root-mean-square* value of a given load effect, when a total of N modes contribute, is given by:

$$W'_j = \frac{\alpha_j \omega_j^4 \overline{a_j^2}}{\left\{ \sum_j^N \alpha_j^2 \omega_j^4 \overline{a_j^2} \right\}^{1/2}} \tag{12.10}$$

It can be demonstrated that equation (12.10) will result in the correct mean square fluctuating response, as given by equation (12.6).

The effective loading distribution for the root mean square fluctuating response, σ_r, obtained by summing over all modes is:

$$p'_{\text{eff}}(x) = m(x)\sum_{j}^{N} W'_j \phi_j(x) \tag{12.11}$$

The total root mean square fluctuating response is then,

$$\sigma_r = \int_0^L p'_{\text{eff}}(x).I(x).dx = \int_0^L I(x).m(x)\sum_{j}^{N} W'_j \phi_j(x).dx$$

$$= \frac{\sum_{j}^{N} \alpha_j^2 \omega_j^4 \overline{a_j^2}}{\left\{\sum_{j}^{N} \alpha_j^2 \omega_j^4 \overline{a_j^2}\right\}^{1/2}} = \left\{\sum_{j}^{N} \alpha_j^2 \omega_j^4 \overline{a_j^2}\right\}^{1/2}$$

which agrees with equation (12.8).

The weighting factor for the contribution from mode j to the effective static loading for the *peak* (maximum or minimum) load effect, r, in a specified time period, T, can be written to a good approximation as:

$$W_j = \frac{\left\{\sum_{j}^{N} \alpha_j^2 g_j^2 \omega_j^4 \overline{a_j^2}\right\}^{1/2} \alpha_j \omega_j^4 \overline{a_j^2}}{\sum_{j}^{N} \alpha_j^2 \omega_j^4 \overline{a_j^2}} \tag{12.12}$$

where g_j is an expected peak factor for the response in mode j.

Equation (12.12) can be obtained from equation (12.10), as follows:

$$W_j = g_r \, W'_j$$

where g_r is the peak factor for the response, which can be approximated quite accurately by,

$$g_r \cong \frac{\left\{\sum_{j}^{N} \alpha_j^2 g_j^2 \omega_j^4 \overline{a_j^2}\right\}^{1/2}}{\left\{\sum_{j}^{N} \alpha_j^2 \omega_j^4 \overline{a_j^2}\right\}^{1/2}} \tag{12.13}$$

This is a weighted average of the peak factors for the various modes.

When only one mode is significant, equation (12.12) reduces to:

$$W_j = g_j \omega_j^2 (\overline{a_j^2})^{1/2} \tag{12.14}$$

i.e. simply the peak inertial force in the mode, j

Note that equation (12.14) is independent of α_j, and hence of the influence line $I(x)$.

The contribution to the total inertial loading from mode j at a given spanwise position is then given by the product of W_j with the mass/unit length, $m(x)$, and the mode shape at that position. The total effective static loading for the peak load effect, r, is then:

$$f_{\text{eff}}(x) = \bar{f}(x) + m(x)\sum_{j}^{N} W_j \phi_j(x) \tag{12.15}$$

The effective static loading depends on the influence line for r through the parameter α_j. Thus the effective static loading will be different for load effects, e.g. bending moments at different spanwise positions. If the influence line is symmetrical about the centre of the bridge, as for example that for the bending moment at centre span, then α_j will be zero for anti-symmetrical modes, i.e only symmetrical modes will contribute.

It should also be noted that since g_r from equation (12.13), can be either positive or negative, the second term on the right-hand-side of equation (12.15) can also be either positive or negative, i.e. it may add or subtract from the mean loading.

12.4 Wind tunnel techniques

The verification of aerodynamic stability and determination of response to wind of long-span bridges, for structural design, is still largely an experimental process, making use of modern wind tunnel techniques. Some of the experimental techniques were discussed in Chapter 7 (Sections 7.6.3 and 7.6.4).

A full wind tunnel test programme for a major long-span bridge might consist of all or some of the following phases.

- Section model tests to determine basic static aerodynamic force and moment coefficients (Section 12.2) for the deck section.
- Section model free or forced vibration tests to determine the aerodynamic or flutter derivatives (Sections 5.5.3 and 12.3.2).
- Section model tests in which the natural frequencies in vertical translation and rotation are scaled to match those of the prototype bridge, and critical flutter speeds are thence determined by slowly increasing the wind-tunnel speed (Section 7.6.3). This may be done in both smooth (low turbulence) and turbulent flow. (An alternative method which better reproduces the mode shapes of the prototype bridge is the 'taut strip' method described in Section 7.6.3).
- Scaled aeroelastic models of the completed bridge, i.e. deck, towers, cables, tested in turbulent boundary-layer flow (Section 7.6.4). The multi-mode aeroelastic modelling scales the various parts of the bridge for elastic properties, mass (inertial), as well as geometric properties. Such tests are quite expensive, with much of the cost in the model design and manufacture.
- Scaled aeroelastic partial models of the bridge in various stages of erection. In most cases, the erection stages find a bridge in its most vulnerable state with respect to wind loading, with lower frequencies making them more prone to turbulent buffeting (Section 12.3.3) and lower flutter speeds, since flutter instabilities tend to occur at constant *reduced* velocity. The erection stage tests may include separate aeroelastic tests of the bridge towers as free-standing structures.

A complete series of tests as outlined above may require two or three different wind tunnels. The wind tunnel testing of bridges tends to be a specialist activity for wind tunnel laboratories, with few facilities being capable of carrying out all the above-listed tests. Some facilities restrict their involvement to section testing for bridge decks; others only carry out boundary-layer wind tunnel tests. However, it should be noted that, to satisfactorily carry out aeroelastic tests on full models of the largest suspension bridges, a test section of at least 10 m width (e.g. Figure 12.7) is required. Few boundary layer wind tunnels are of this size.

12.5 Vibration of bridge cables

As the spans of cable-stayed bridges have increased and the cables themselves have become longer, cable vibration has become more of a problem. One of the more interesting excitation mechanisms, and until recently, least-understood ones, is the so-called 'rain-wind' vibration. In the following sections, the history of occurrences of this phenomenon, suggested excitation mechanisms, and methods of mitigating the vibrations, are reviewed.

12.5.1 Rain-wind vibration

The first, clearly defined, occurrence of wind-induced cable vibration, during which the presence of rain was an essential feature, was observed during the construction of Meiko-Nishi Bridge at Nagoya Harbour, Japan, in 1984. Low frequency (1–3 Hz) vibrations of some cables, with double amplitudes up to 300 mm, were observed, over a 5-month period. This bridge has a main span of 405 m with cables up to 165 mm in diameter, and lengths varying from 65 to 200 m. The vibrations occurred in wind speeds between 7 and 14 m/s; these speeds greatly exceeded the critical wind speeds for vortex shedding at the low

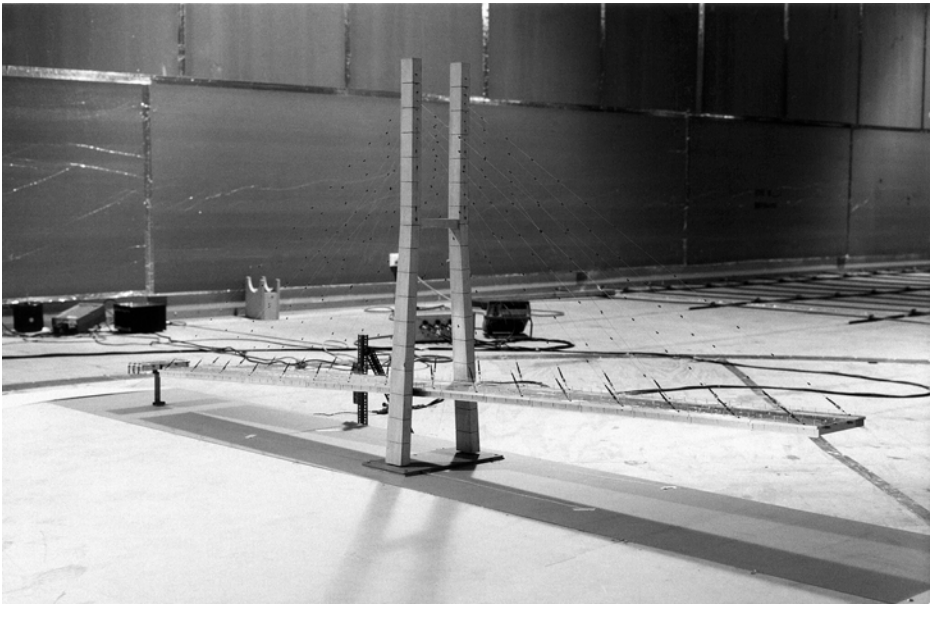

Figure 12.7 A full aeroelastic model of a cable-stayed bridge in a construction stage.

frequencies observed. Using a section of polyethylene pipe casing from the prototype structure, wind tunnel tests were conducted, with and without simulated rain, and it was clearly established that the rain was necessary to induce vibration over a defined range of wind speeds (Hikami and Shiraishi, 1988).

Later, it was found that rain-wind induced vibration had occurred on six bridges in Japan. A common feature was that the vibrating cables were usually sloping downwards in a downwind direction, with the wind approaching obliquely to the plane of the cable (Figure 12.8). Vibrations were apparently observed only for cables encased in polyethylene.

Outside Japan, rain-wind vibration of bridge cables have been observed on the Faroe Bridge (Denmark), Bretonne Bridge (France), the Koehlbrand Bridge (Germany) and Normandie Bridge (France). Many other bridges have, experienced cable vibrations – some from different mechanisms such as high-frequency vortex-shedding excitation, or from unknown or undefined mechanisms.

12.5.2 Excitation mechanisms

The wind-tunnel studies carried out following the vibrations observed on the Meiko-Nishi Bridge, indicated that the motion was induced by the presence of two water 'rivulets', that oscillated in circumferential position with the cable motion. At low wind speeds, a single rivulet formed on the underside. Motion commenced at higher wind speeds when a second rivulet formed on the upper surface. The rivulets act as trigger points to promote flow separation on the vibrating cable, as shown in Figure 12.9. In this figure, the effective cross-wind shape is postulated to be elliptical. Other observations have suggested that the circumferential motion was not two-dimensional, and that the width and depth of the rivulet on the upper surface was less than that on the lower surface.

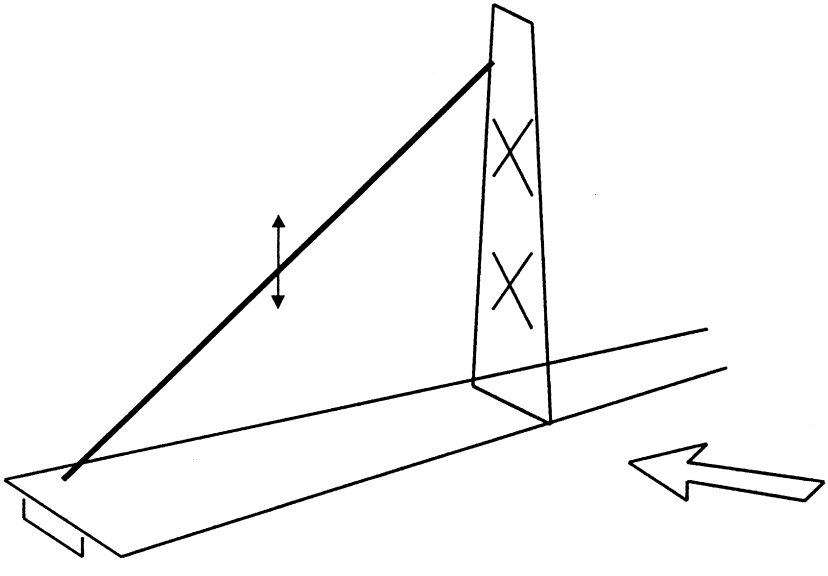

Figure 12.8 Typical cable/wind orientation for rain-wind vibration (Matsumoto *et al.*, 1993).

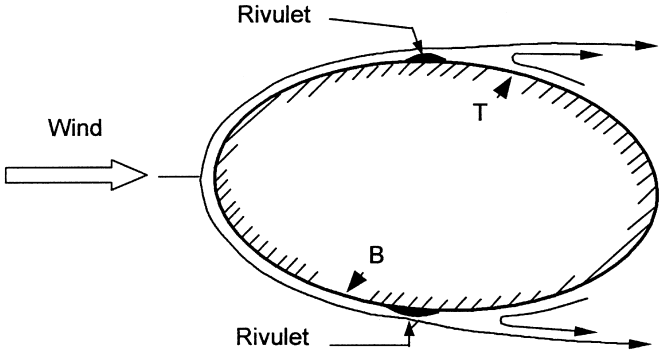

Figure 12.9 Flow separations produced by rivulets of rain water.

Wind tunnel tests in France for the Normandie Bridge (Flamand *et al.*, 1994) showed that carbon combustion products deposited on the surface of the casing were necessary for aerodynamic instability to occur, indicating the role played by surface tension in allowing the water rivulet to be maintained.

Fundamental wind tunnel model studies of inclined cable aerodynamics, with and without rain, have been made at various angles of pitch (inclination), yaw and rivulet position. It was found that aerodynamic oscillations of either the 'velocity-restricted' type (i.e. occurring over a narrow range of wind speeds) and produced by vortex shedding, or of the 'divergent' or galloping type (Section 5.5.2) – i.e. vibration triggered at a particular wind speed, and rapidly increasing in amplitude). However, instabilities usually commenced at reduced wind velocity ($U/n_c b$, where U is the wind velocity, n_c is the cable frequency and b is the diameter) of about 40. In the case of the vortex-induced vibrations, these tended to occur in narrow bands of wind speed centred around 40 or multiples of 40, i.e. 80, 120, etc. (Matsumoto *et al.,* 1993).

12.5.3 Solutions

The solutions that have been successful in eliminating, or mitigating rain-wind induced vibration of bridge cables can be divided into the following categories:

- Aerodynamic treatments, i.e. geometrical modifications of the outer cable casing
- Auxiliary cable ties
- Auxiliary dampers

Model measurements were carried out by Miyata *et al.* (1994), on sections of cable models with the same diameter as full-size cables, with a variety of roughened surface treatments (Figure 12.10). Discrete roughness, of about 1% of the diameter, was found to be effective in suppressing rain-wind induced vibration. The explanation was that supercritical flow was promoted at lower Reynolds numbers than would occur on cables with smooth surface finish.

Wind tunnel tests in France (Flamand, 1994), found that parallel surface projections did stabilize a cable model, but produced a high drag coefficient in the supercritical Reynolds number range. An alternative solution which minimized the drag increase, was adopted,

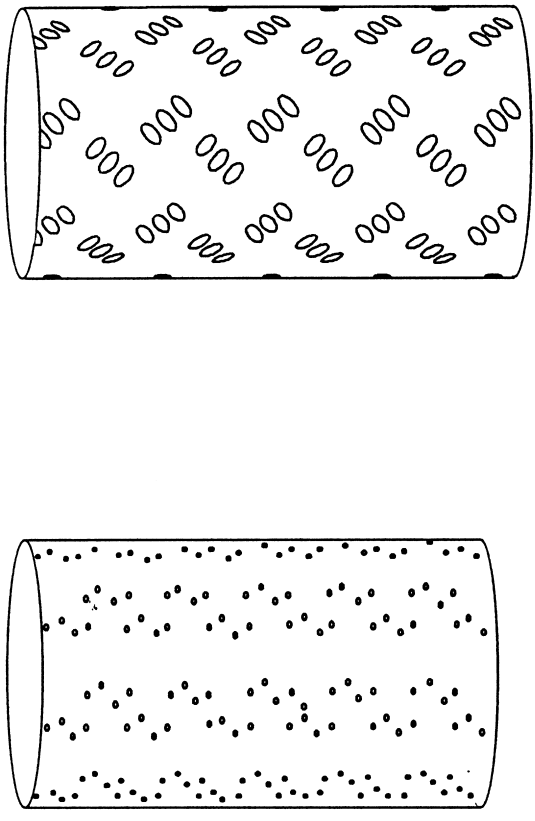

Figure 12.10 Surface roughness treatments for cable vibration mitigation (Miyata *et al.*, 1994).

namely the use of a double helix spiral, 1.3 mm high, 2 mm wide, and with a pitch of 0.6 m. This configuration was adopted for the Normandie Bridge.

Usually only one or two stay cables from a harp or fan array, will experience rain-wind vibration in particular atmospheric conditions. This observation led to a solution that has been used on several bridges – cable cross-ties. They have also been used on the Normandie Bridge (currently the world's longest cable-stayed type), where they are known as 'aiguilles'. They have been adopted for the Dane Point Bridge, Florida, U.S.A., and for the Tatara Bridge, Japan (Figure 12.11).

A fundamental study of damping in stay cables, and of the effectiveness of cross ties, was carried out by Yamaguchi and Fujino (1994). Measurements on cables of a typical cable-stayed bridge indicated a range of critical damping ratios, from about 0.001 to 0.003, for the first mode, with lower values occurring for the low sag ratios, i.e. a higher prestress. A laboratory experiment on cross ties showed that a 'stiff' cross tie performed a function of transferring vibration energy from a vibrating cable to its neighbours. By use of 'soft' cross ties, energy could also be dissipated in the cross ties, making this system more effective.

Energy dissipation can also be provided by auxiliary damping devices mounted between the cable and the bridge girder, near the connection points. This solution is more expensive

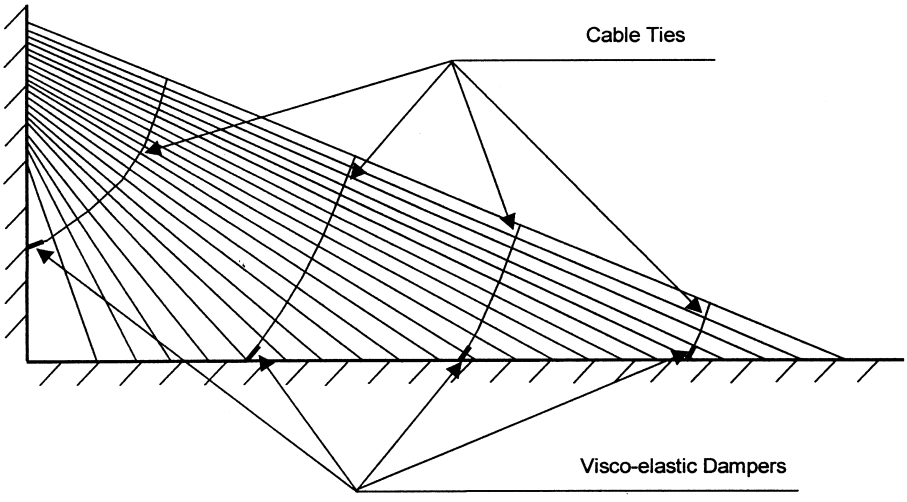

Figure 12.11 Vibration mitigation cable ties used on the Tatara Bridge.

than the cross-tie method, but more aesthetically pleasing. Oil dampers and visco-elastic dampers (Section 9.9.2) have been used for this purpose.

12.6 Case studies

The literature on the aerodynamics of long-span bridges is extensive, and many papers on the subject contain references to particular bridges for illustration purposes. Sections 12.3.1 and 12.5 contain several examples in relation to vortex-shedding induced vibrations and cable vibrations, respectively. Holmes (1999) has described the application of the equivalent static load method (Section 12.3.4) to generate design loadings for the Baram River (Malaysia) cable-stayed bridge.

The extensive wind engineering studies carried out for the current (2000) first and second longest bridges in the world, are described by Miyata *et al.* (1992) for the Akashi Kaikyo Bridge, and by Reinhold *et al.* (1992) and Larsen and Jacobsen (1992) for the Great Belt East Bridge (Denmark). The wind design of the Normandie Bridge from the designer's point of view is well covered by Virlogeux (1992).

12.7 Summary

In this chapter, the aerodynamics of bridges have been presented in a summary form. Long-span bridges are probably the most 'wind-sensitive' of all structures, and their aerodynamics are complex and the sphere of specialists. The main phenomena of vortex shedding, flutter and buffeting have been discussed.

The vibration of the cables on cable-stayed bridges has become the limiting factor on their ultimate spans, and this topic, with alleviation measures, has been discussed in some detail.

References

Baker, B. (1884) 'The Forth Bridge', *Engineering* 38: 213.

Billington, D. P. (1977) 'History and esthetics in suspension bridges', *A.S.C.E. Journal of the Structural Division* 103: 1655–72.

Davenport, A. G. (1962) 'Buffeting of a suspension bridge by storm winds', *A.S.C.E. Journal of the Structural Division* 88: 233–68.

Flamand, O. (1994) 'Rain-wind induced vibrations of cables', *International Conference on Cable-stayed and Suspension Bridges*, Deauville, France, 12–15 October.

Frandsen, J. B. (2001) 'Simultaneous pressures and accelerations measured full-scale on the Great Belt East suspension bridge', *Journal of Wind Engineering and Industrial Aerodynamics* 89: 95–129.

Ge, Y. J. and Tanaka, H. (2000) 'Aerodynamic flutter analysis of cable-supported bridges by multi-mode and full-mode approaches', *Journal of Wind Engineering and Industrial Aerodynamics* 86: 123–53.

Gimsing, N. J. (1983) *Cable-Supported Bridges*. John Wiley.

Hikami, Y. and Shiraishi, N. (1988) 'Rain-wind induced vibrations of cables in cable-stayed bridges', *Journal of Wind Engineering and Industrial Aerodynamics* 29: 409–18.

Holmes, J. D. (1975) 'Prediction of the response of a cable-stayed bridge to turbulence', *Proceedings, 4th International Conference on Wind Effects on Buildings and Structures*, London, 8–12 September, Cambridge University Press, 187–97.

—— (1979) 'Monte Carlo simulation of the wind-induced response of a cable-stayed bridge', *Proceedings, 3rd International Conference on Applications of Statistics and Probability in Soil and Structural Engineering (ICASP-3)*, Sydney, University of New South Wales, 551–65.

—— (1999) 'Equivalent static load distributions for resonant dynamic response of bridges', *Proceedings, 10th International Conference on Wind Engineering*, Copenhagen, 21–24 June, Rotterdam: A.A. Balkema, 907–11.

Irwin, H. P. A. H. (1977) 'Wind tunnel and analytical investigations of the response of Lions' Gate Bridge to a turbulent wind', National Aeronautical Establishment, Canada. Laboratory Technical Report, LTR-LA-210, June 1977.

Jancauskas E. D. (1986) 'The aerodynamic admittance of two-dimensional rectangular section cylinders in smooth flow', *Journal of Wind Engineering Industrial Aerodynamics* 23: 395–408.

Kernot, W. C. (1893) 'Wind pressure', *Proceedings, Australasian Society for the Advancement of Science* V: 573–81.

Konishi, I., Shiraishi, N. and Matsumoto, M. (1975) 'Aerodynamic response characteristics of bridge structures', *Proceedings, 4th Internal Conference on Wind Effects on Buildings and Structures*, London, 8–12 September, Cambridge University Press, 199–208.

Larsen, A. (ed.) (1992) 'Aerodynamics of large bridges', *Proceedings of the First International Symposium on Aerodynamics of Large Bridges,* Copenhagen, Denmark, 19–21 February, 1992, Rotterdam: A.A. Balkema.

Larsen, A. and Jacobsen, A. S. (1992) 'Aerodynamic design of the Great Belt East Bridge', *Proceedings of the First International Symposium on Aerodynamics of Large Bridges,* Copenhagen, Denmark, 19–21 February, 1992, Rotterdam: A.A. Balkema, 269–83.

Larsen, A., Esdahl, S., Andersen, J. E. and Vejrum, T. (1999) 'Vortex shedding excitation of the Great Belt suspension bridge', *Proceedings, 10th International Conference on Wind Engineering*, Copenhagen, 21–24 June, Rotterdam: A.A. Balkema, 947–54.

Matsumoto, M., Shirato, H., Saito, H., Kitizawa, H. and Nishizaki, T. (1993) 'Response characteristics of rain-wind induced vibration of stay cables of cable-stayed bridges', *1st. European-African Regional Congress on Wind Engineering*, Guernsey, 20–24 September.

Melbourne, W. H. (1979) 'Model and full-scale response to wind action of the cable-stayed, box-girder, West Gate Bridge', *IAHR/IUTAM Symposium on Flow-Induced Vibrations*, Karlsruhe, Germany, September 3–8.

Miyata, T., Yamada, H. and Hojo, T. (1994) 'Aerodynamic response of PE stay cables with pattern indented surface', *International Conference on Cable-stayed and Suspension Bridges*, Deauville, France, 12–15 October.

Miyata, T., Yokoyama, Y., Yasuda, M. and Hikami, Y. (1992) 'Akashi Kaikyo Bridge: wind effects and full model tests', *Proceedings of the First International Symposium on Aerodynamics of Large Bridges,* Copenhagen, Denmark, 19–21 February, 1992, Rotterdam: A.A. Balkema, 217–36.

Ostenfeld, K. H. and Larsen, A. (1992) 'Bridge engineering and aerodynamics', *Proceedings of the First International Symposium on Aerodynamics of Large Bridges,* Copenhagen, Denmark, 19–21 February, 1992, Rotterdam: A.A. Balkema, 3–22.

Petroski, H. (1996) *Engineers of Dreams*, New York: Vintage Books.

Reinhold, T. A., Brinch, M. and Damsgaard, A. (1992) 'Wind-tunnel tests for the Great Belt link', *Proceedings of the First International Symposium on Aerodynamics of Large Bridges,* Copenhagen, Denmark, 19–21 February, 1992, Rotterdam: A.A. Balkema, 255–67.

Sabzevari, A. and Scanlan, R. H. (1968) 'Aerodynamic instability of suspension bridges', *A.S.C.E. Journal of the Engineering Mechanics Division* 94: 489–519.

Selberg, A. (1963) 'Aerodynamic effects on suspension bridges', *Proceedings, International Conference on Wind Effects on Buildings and Structures*, Teddington, U.K. 26–28 June, 462–86.

Scanlan, R. H. and Gade, R. H. (1977) 'Motion of suspended bridge spans under gusty winds', *A.S.C.E. Journal of the Strucural Division* 103: 1867–83.

Scanlan, R. H. and Lin, W.-H. (1978) 'Effects of turbulence on bridge flutter derivatives', *A.S.C.E. Journal of the Engineering Mechanics Division* 104: 719–33.

Scanlan, R. H. and Tomko, J. J. (1971) 'Airfoil and bridge flutter derivatives', *A.S.C.E. Journal of the Engineering Mechanics Division* 97: 1717–37.

Shiraishi, N. and Matsumoto, M. (1977) 'Aerodynamic responses of bridge structures subjected to strong winds', *Symposium on Engineering for Natural Hazards,* Manila, September.

Simiu, E. and Scanlan, R. H. (1996) *Wind Effects on Structures – Fundamentals and Applications to Design,* third edn. New York: John Wiley.

Smith, I. J. (1980) 'Wind induced dynamic response of the Wye Bridge', *Engineering Structures* 2: 202–8.

Steinman, D. B. and Watson, S. R. (1957) *Bridges and their Builders*, New York: Dover.

van Nunen, J. W. G. and Persoon, A. J. (1982) 'Investigation of the vibrational behaviour of a cable-stayed bridge under wind loads', *Engineering Structures* 4: 99–105.

Virlogeux, M. (1992) 'Wind design and analysis for the Normandy Bridge', *Proceedings of the First International Symposium on Aerodynamics of Large Bridges,* Copenhagen, Denmark, 19–21 February, 1992, Rotterdam: A.A. Balkema, 183–216.

—— (1999) 'Recent evolution of cable-stayed bridges', *Engineering Structures* 21: 737–55.

Wardlaw, R. L. (1971) 'Some approaches for improving the aerodynamic stability of bridge road decks', *3rd International Conference on Wind Effects on Buildings and Structures*, Tokyo, Japan, September 6–9, Tokyo: Saikon Shuppan.

Yamaguchi, H. and Fujino, T. (1994) 'Damping in cables in cable-stayed bridges with and without damping control measures', *International Conference on Cable-stayed and Suspension Bridges*, Deauville, France, 12–15 October.